Leakage current reduction by thermal oxidation in Ni/Au Schottky contacts on lattice-matched $In_{0.18}Al_{0.82}N$/GaN heterostructures*

Lin Fang(林 芳)[a)†], Shen Bo(沈 波)[a)], Lu Li-Wu(卢励吾)[a)],
Xu Fu-Jun(许福军)[a)], Liu Xin-Yu(刘新宇)[b)], and Wei Ke(魏 珂)[b)]

[a)] *State Key Laboratory of Artificial Microstructure and Mesoscopic Physics, School of Physics, Peking University, Beijing* 100871, *China*
[b)] *Institute of Microelectronics of Chinese Academy of Sciences, Beijing* 100029, *China*

(Received 9 May 2013; revised manuscript received 29 July 2013; published online 24 January 2014)

By using temperature-dependent current–voltage, variable-frequency capacitance–voltage, and Hall measurements, the effects of the thermal oxidation on the electrical properties of Ni/Au Schottky contacts on lattice-matched $In_{0.18}Al_{0.82}N$/GaN heterostructures are investigated. Decrease of the reverse leakage current down to six orders of magnitude is observed after the thermal oxidation of the $In_{0.18}Al_{0.82}N$/GaN heterostructures at 700 °C. It is confirmed that the reverse leakage current is dominated by the Frenkel–Poole emission, and the main origin of the leakage current is the emission of electrons from a trap state near the metal/semiconductor interface into a continuum of electronic states associated with the conductive dislocations in the $In_xAl_{1-x}N$ barrier. It is believed that the thermal oxidation results in the formation of a thin oxide layer on the $In_xAl_{1-x}N$ surface, which increases the electron emission barrier height.

Keywords: leakage current, thermal oxidation, Frenkel–Poole emission

PACS: 73.40.Kp, 73.61.Ey **DOI:** 10.1088/1674-1056/23/3/037303

1. Introduction

The lattice-matched $In_{0.18}Al_{0.82}N$/GaN heterostructures have recently aroused great interest as an ideal candidate for high-temperature, high-frequency, and high power applications.[1–3] The $In_{0.18}Al_{0.82}N$/GaN high electron mobility transistor (HEMT), which leads to a stress-free structure, represents an alternative to the $Al_xGa_{1-x}N$/GaN HEMT with a high density of the two-dimensional electron gas (2DEG) and high reliability.[1,2] However, many important problems facing the $In_{0.18}Al_{0.82}N$/GaN HEMTs are still not resolved, such as the high reverse leakage current of the Schottky contacts and charges trapped in the $In_xAl_{1-x}N$ barrier.[3–5] Several investigations have shown that the effects of both dislocations and defect states in the barrier might play an important role in reverse leakage current.[4–6] Arslan *et al.*[4] analyzed the leakage current mechanisms in the Schottky contacts on lattice-matched $In_xAl_{1-x}N$/AlN/GaN heterostructures and concluded that the Frenkel–Poole (F–P) emission dominates from 250 K to 375 K. They thought that the main process in the leakage flow is the emission of electrons from a trapped state near the metal/semiconductor (M/S) interface into a continuum of states associated with conductive dislocations. Chikhaoui *et al.*[5] furthermore gave a description of the F–P emission with the determination of the trap and dislocation energy level. However, to date, no effective methods of leakage current reduction have been achieved.

In the present study, by using temperature-dependent current–voltage (I–V), variable-frequency capacitance–voltage (C–V), and Hall measurements, we demonstrate a significant improvement in the leakage current of Ni/Au Schottky contacts on lattice-matched $In_{0.18}Al_{0.82}N$/GaN heterostructures after thermal oxidation.

2. Experiments

The $In_{0.18}Al_{0.82}N$/GaN heterostructures were grown on the (0001) surface of a sapphire substrate using metal–organic chemical vapor deposition (MOCVD). The growth was initiated with a 25 nm-thick low-temperature GaN nucleation layer. Then, an approximately 2.0 μm GaN template was grown at 1070 °C followed by a 20 nm-thick $In_{0.18}Al_{0.82}N$ barrier layer grown at 800 °C. The typical mobility and density of the 2DEG in the heterostructures at room temperature (RT) are 1180 $cm^2 \cdot V^{-1} \cdot s^{-1}$ and 2.31×10^{13} cm^{-2}, respectively.

After the MOCVD growth, the van der Pauw configurations and Schottky diode structures were fabricated. Ti/Al/Ti/Au (20/180/55/50 nm) Ohmic contacts were deposited, followed by rapid thermal annealing in N_2 ambient at 850 °C for 30 s. Then, a 500 nm-thick top layer of Au patterned with a second lithography was deposited to improve the resistance to oxidation of the Ohmic contacts during high temperature annealing. The samples were annealed in O_2 ambient for 1 h at 600 °C (600 °C-annealed) and 700 °C (700 °C-annealed), respectively. Finally, Ni/Au (50/100 nm) were deposited as Schottky contacts. The samples without the thermal

*Project supported by the National Natural Science Foundation of China (Grant Nos. 60444007, 11174008, 60325413, and 10774001).
†Corresponding author. E-mail: linfang@pku.edu.cn
© 2014 Chinese Physical Society and IOP Publishing Ltd

oxidation were also prepared for reference (non-annealed).

The RT 2DEG mobility and density for the 700 °C-annealed sample are 1180 $cm^2 \cdot V^{-1} \cdot s^{-1}$ and 1.83×10^{13} cm^{-2}, respectively. Compared with the non-annealed sample, the sample after thermal oxidation has a slight reduction of 2DEG density, and the 2DEG mobility always remains unchanged. To identify the quality of the Ohmic contact of the sample, the specific contact resistivity is determined by the linear transmission line method (LTLM). The values of the specific contact resistivity are 1.39×10^{-5} $\Omega \cdot cm^2$ and 6.44×10^{-5} $\Omega \cdot cm^2$ for the non-annealed sample and 700 °C-annealed sample, respectively, which indicates the thermal oxidation has little influence on the Ohmic contact resistivity.

3. Results and discussion

Figure 1 shows the curves of current density versus bias voltage for non-annealed, 600 °C-annealed, and 700 °C-annealed samples at RT, respectively. The thermal oxidation of bare $In_{0.18}Al_{0.82}N$/GaN heterostructures at 700 °C leads to a significant decrease of the reverse leakage current down to six orders of magnitude. The significant decrease in reverse leakage current is also accompanied by a little decrease in forward current. The forward *I*–*V* characteristics are analyzed using the standard thermionic emission (TE) model[7] under the assumption of an effective Richardson constant of $A^* = 56$ $A \cdot cm^{-2} \cdot K^{-2}$.[8] The non-annealed sample displays a low Schottky barrier height (SBH) of $\Phi_b = 1.2$ eV and a high ideality factor (IF) of $n = 2.9$. The 600 °C-annealed and 700 °C-annealed samples exhibit SBH values of 1.7 and 1.8 eV and IF values of 1.3 and 1.9, respectively. The thermal oxidation increases the SBH accompanied with an improvement in IF. Lin *et al.*[9] analyzed the effects of a thin native oxide layer on a Au/Ni/n-type GaN Schottky diode and concluded that the tunneling current was induced in the presence of native oxide on the GaN surface. As a result, the forward *I*–*V* characteristics for the 700 °C-annealed sample in our work have also been analyzed using the thermionic field emission (TFE) model.[9] However, the 700 °C-annealed sample demonstrates nearly the same SBH in the TFE model (1.754 eV) as in the TE model (1.775 eV). An increase of the series resistance should be responsible for a little decrease in forward current after the thermal oxidation. The specific contact resistivity increases from 1.39×10^{-5} $\Omega \cdot cm^2$ to 6.44×10^{-5} $\Omega \cdot cm^2$ after the thermal oxidation at 700 °C without a change in magnitude. As a result, the increase of the series resistance of the diode should not be the main cause for the decrease of the reverse leakage current after the thermal oxidation.

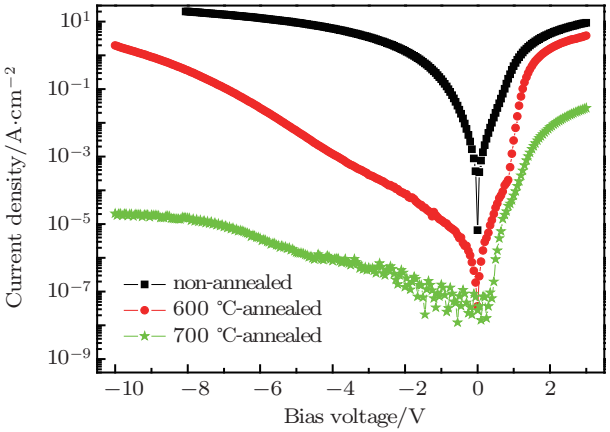


Fig. 1. (color online) Curves of current density versus bias voltage for non-annealed, 600 °C-annealed, and 700 °C-annealed samples at RT, respectively.

The surface chemistry properties of the $In_xAl_{1-x}N$ surfaces for non-annealed and 700 °C-annealed samples are studied by x-ray photoemission spectroscopy (XPS) as shown in Fig. 2. From the O 1s XPS spectra, it can be seen that a few O–H bonds (531.2 eV) exist on the non-annealed $In_xAl_{1-x}N$ surface while O–In (529.7 eV) and a few O–H bonds (531.2 eV) exist on the 700 °C-annealed $In_xAl_{1-x}N$ surface.[10] Therefore, we can deduce that the thermal annealing in O_2 ambient introduces a thin oxide layer on the $In_xAl_{1-x}N$ surface as a dielectric.

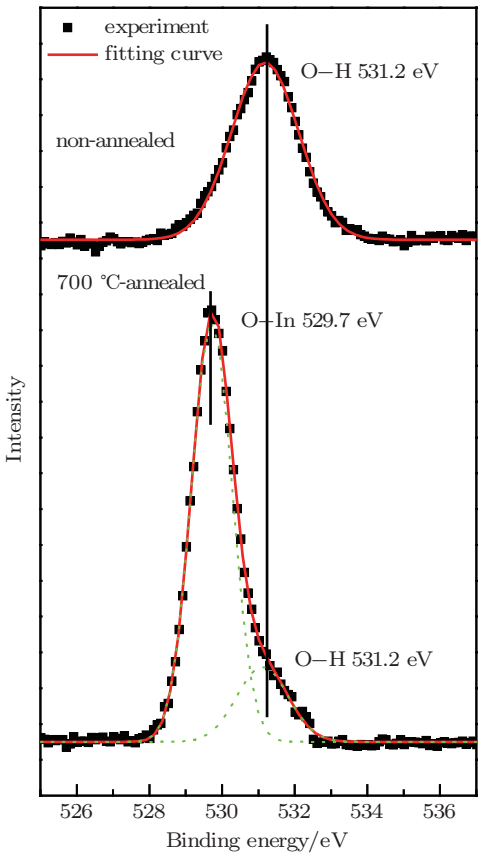


Fig. 2. (color online) XPS spectra from O 1s core level of the $In_xAl_{1-x}N$ surfaces for non-annealed and 700 °C-annealed samples, respectively. Dashed lines correspond to fitted curves for each bond.

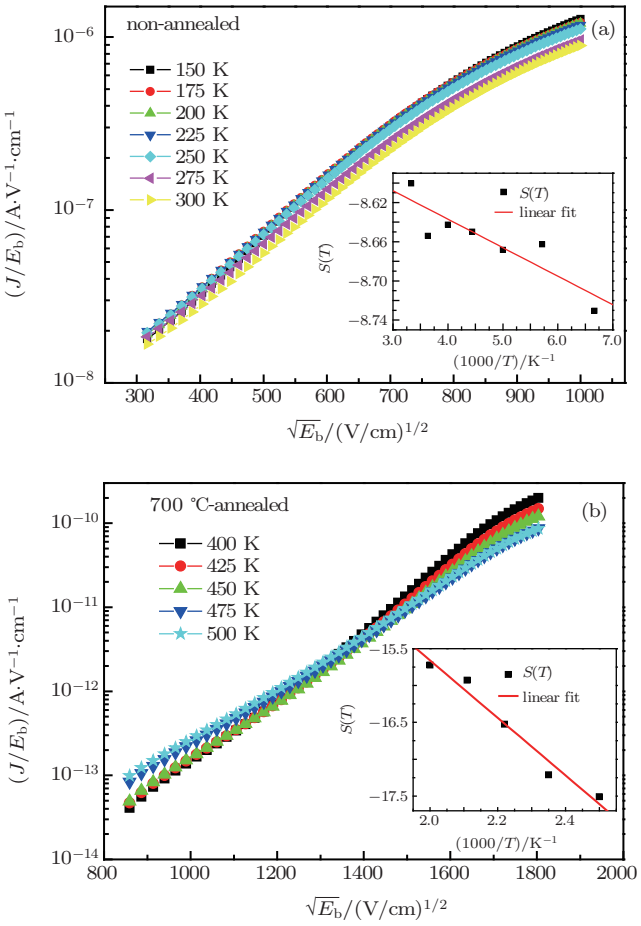


Fig. 3. (color online) Measured curves of reverse leakage current density divided by electric field versus square root of electric field for (a) non-annealed and (b) 700 °C-annealed samples, respectively. The insets show the plots of $S(T)$ versus $1000/T$ which allows the determination of emission barrier height.

The F–P emission refers to the electric-field-enhanced thermal emission from a trapped state into a continuum of electronic states. The reverse leakage current density J associated with the F–P emission is given by[4–6]

$$J = CE_b \exp[-q(\Phi_t - \sqrt{qE_b/\pi\varepsilon_0\varepsilon_s})/kT],$$

where E_b is the electric field in the $In_xAl_{1-x}N$ barrier at the metal/$In_xAl_{1-x}N$ interface for the non-annealed sample or at the thin oxide/$In_xAl_{1-x}N$ interface for the 700 °C-annealed sample, Φ_t is the barrier height for electron emission from the trapped states, ε_s is the relative dielectric permittivity, ε_0 is the permittivity of free space, T is the absolute temperature, and k is the Boltzmann constant. For the current transport dominated by F–P emission, the $\ln(J/E_b)$ should be a linear function of $\sqrt{E_b}$ as follows: $\ln(J/E_b) = R(T)\sqrt{E_b} + S(T)$, with $R(T) = q\sqrt{q/(\pi\varepsilon_0\varepsilon_s)}/kT$, and $S(T) = -q\Phi_t/(kT) + \ln C$. The measured reverse leakage current densities in the non-annealed samples from 150 K to 300 K and the 700 °C-annealed samples from 400 K to 500 K are observed to be dependent on both electric field and temperature which are expected to be of F–P emission, which are shown in Figs. 3(a) and 3(b). The inset shows the plot of $S(T)$ versus $1000/T$ which allows the determination of emission barrier height. We obtain $\Phi_t = 0.003$ eV from 150 K to 300 K for the non-annealed sample and $\Phi_t = 0.30$ eV, $\Phi_t = 0.34$ eV from 400 K to 500 K for the 600 °C-annealed and the 700 °C-annealed samples, respectively. The thermal oxidation leads to the increase of emission barrier height.

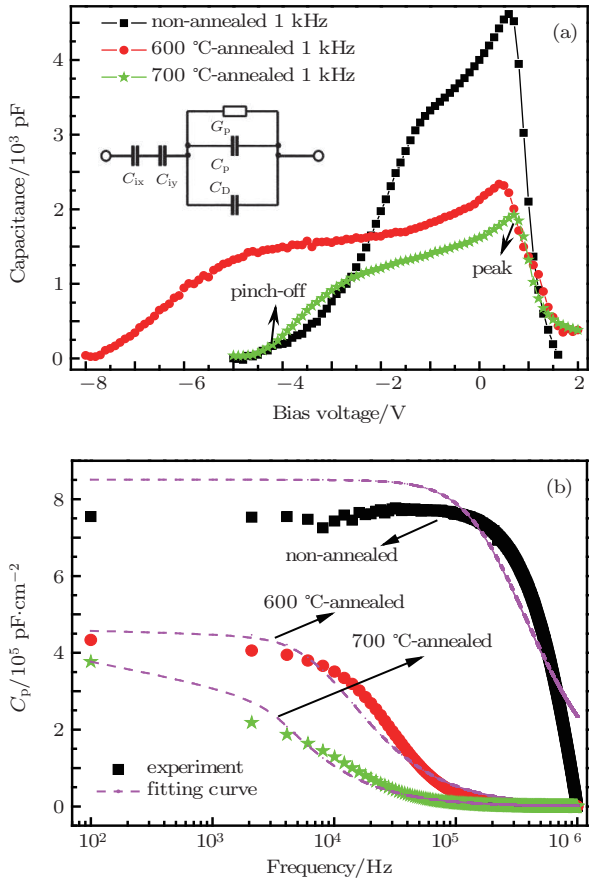


Fig. 4. (color online) (a) Measured curves of device capacitance C_M versus bias voltage for non-annealed, 600 °C-annealed, and 700 °C-annealed samples at 1 kHz, respectively. The inset shows the full equivalent circuit model employed in our analysis. (b) The frequency dependences of the values of interface state capacitance C_p for non-annealed, 600 °C-annealed, and 700 °C-annealed samples, respectively, the voltage V is selected to be at pinch-off voltage. Dashed lines correspond to the best fitted curves for the experimental results.

Figure 4(a) shows the measured values of device capacitance C_M versus bias voltage for non-annealed, 600 °C-annealed, and 700 °C-annealed samples at 1 kHz, respectively. A clear 2DEG plateau region and a carrier accumulation region in the C–V curves can be observed. The negative bias voltage value after the complete depletion of the 2DEG (pinch-off) and the positive bias voltage value before the diode turns on in the carrier accumulation region (peak) are indicated for the 700 °C-annealed sample by the arrows in Fig. 4(a). The sheet carrier densities are determined by the integration of the C–V curves, and we obtain 2.36×10^{13} cm^{-2}, 2.28×10^{13} cm^{-2}, and 1.98×10^{13} cm^{-2} for the non-annealed, 600 °C-annealed, and 700 °C-annealed samples, respectively.

After the oxidation at 600 °C the pinch-off voltage shifts towards −7 V as a result of the formation of a thin oxide layer on the $In_xAl_{1-x}N$ surface. After the oxidation at 700 °C the pinch-off voltage returns to −4 V as a result of the reduction of the sheet carrier density. Figure 4(b) shows the frequency dependence of the interface state capacitance C_p for the non-annealed, 600 °C-annealed, and 700 °C-annealed samples, respectively. The voltage V is selected to be the pinch-off voltage. Measurements of the device capacitance C_M as functions of frequency f ranging from 100 Hz to 1 MHz are performed. The full equivalent circuit model employed in our analysis is shown in the inset of Fig. 4(a), where C_{ix} is the oxide layer capacitance, C_{iy} the $In_xAl_{1-x}N$ barrier capacitance, C_p the interface state equivalent capacitance, G_p the interface state equivalent conductance, and C_D the depletion region capacitance. The analysis is performed on the assumption that the interface states comprise a continuum of levels. C_p is given by[11–13] $C_p = q^2AN_{ss}\arctan(\omega\tau)/(\omega\tau)$, where ω is the circular frequency of the test signal, τ the time constant of the interface state, A the contact area, N_{ss} the density of interface states. At the pinch-off voltage, we can obtain C_p by $C_p = C_i[(C_i/C_M - 1)^{-1} - (C_i/C_M(HF) - 1)^{-1}]$, where $1/C_i = 1/C_{ix} + 1/C_{iy}$ and $C_M(HF)$ is the high-frequency capacitance. At peak voltage, we can obtain C_p i.e., $C_p = C_M - C_M(HF)$. The interface state capture cross section σ_n is given by $\sigma_n = (\tau v_{th}N_D)^{-1}\exp(-qV_s/kT)$, where v_{th} is the thermal velocity of electrons, N_D the ionized impurity concentration, V_s the semiconductor surface potential.[14] The interface state energy level is given by $E_C - E_T = q(V_s + V_B)$, where V_B is the potential difference between the conduction-band edge and the Fermi level, and we obtain $qV_B = 0.02$ eV from the temperature-dependent Hall measurements. By plotting C_p versus $f(C-f)$ and fitting the resulting curves to C_p equations, N_{ss} and τ can be extracted. Based on the work by Soh *et al.*,[15] σ_n for O_N related defect clusters along the dislocation line is 1.8×10^{-17} cm^2, and then we can obtain V_s and $E_C - E_T$.[15] At peak voltage, the C–f characteristics are corresponding to the characteristics of interface states located at the M/S interface. However, the C–f characteristics at the pinch-off voltage are not exactly the characteristics of an interface effect. They can be best described as the characteristics of the overall effect including the real interface states at the $In_xAl_{1-x}N$/GaN interface and the defect states inside the $In_xAl_{1-x}N$ barrier (near-interface states). As a result, the V_s at pinch-off voltage is not exactly equal to the usual semiconductor surface potential (the potential difference between the semiconductor surface and the semiconductor interior, the bending degree of the GaN conduction band here), and the V_s can be considered as a quasi-semiconductor surface potential associated with near-interface states. In this work, we put an emphasis on the identification of the defect states associated with the conductive dislocations inside the $In_xAl_{1-x}N$ barrier by C–f analysis of the Schottky diodes at the pinch-off voltage.

Table 1 shows the simulation results of the defect states located at the M/S interface and inside the $In_xAl_{1-x}N$ barrier for the non-annealed, 600 °C-annealed, and 700 °C-annealed samples, respectively. Thermal oxidation does not induce the increase of the surface state density on the $In_xAl_{1-x}N$ surface. A continuum of electronic states located inside the $In_xAl_{1-x}N$ barrier with an activation energy of about 1.16 eV and a density of 2.36×10^{12} cm^{-2}·eV^{-1} are determined for 700 °C-annealed sample compared with an activation energy of about 1.02 eV and a density of 5.32×10^{12} cm^{-2}·eV^{-1} before the thermal oxidation. The decrease of the defect state density associated with the conductive dislocations in the $In_xAl_{1-x}N$ barrier after the thermal oxidation may also be responsible for the reverse leakage current reduction.

Figure 5 shows the schematic energy-band diagrams of Ni/Au Schottky contacts on the $In_{0.18}Al_{0.82}N$/GaN heterostructures before and after the thermal oxidation. We suggest that the reverse leakage current in the Schottky contact is dominated by F–P emission, and the main source of the leakage current is the emission of electrons from a trapped state within the semiconductor (most likely a trapped state near the M/S interface) into a continuum of electronic states associated with the conductive dislocations. In this model, the trapped state energy must be close to the metal Fermi level, and the emission of carriers from the metal into the trapped states would easily occur. The analyses of F–P emission and C–f characteristics indicate that the increase of the emission barrier height and the decrease of the defect state density associated with the conductive dislocations in the $In_xAl_{1-x}N$ barrier by the thermal oxidation should be the causes of the observed device improvement. It is believed that the thermal oxidation results in the formation of a thin oxide layer on the $In_{0.18}Al_{0.82}N$ surface, which increases the emission barrier height.

Table 1. Simulation results of the interface state density N_{ss} and the interface state energy level $E_C - E_T$ located at the M/S interface and inside the $In_xAl_{1-x}N$ barrier for non-annealed, 600 °C-annealed, and 700 °C-annealed samples, respectively.

	Inside the $In_xAl_{1-x}N$ barrier		At the M/S interface	
	$E_C - E_T$/eV	$N_{ss}/10^{12}$ cm^{-2}·eV^{-1}	$E_C - E_T$/eV	$N_{ss}/10^{12}$ cm^{-2}·eV^{-1}
Non-annealed	1.023	5.32	0.118	4.13
600 °C-annealed	1.131	2.86	0.214	3.31
700 °C-annealed	1.158	2.36	0.254	3.11

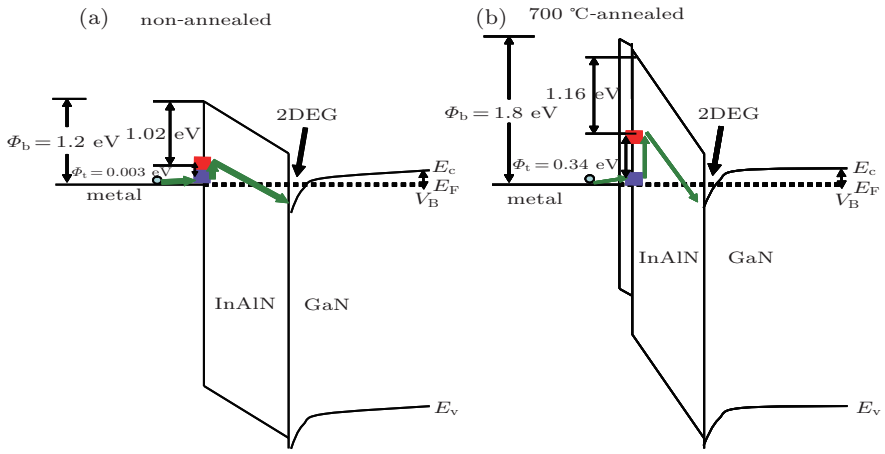


Fig. 5. (color online) Schematic energy-band diagrams of the Au/Ni/$In_{0.18}Al_{0.82}N$/GaN Schottky diodes before (a) and after (b) the thermal oxidation, respectively.

4. Conclusions

In the present paper, by using temperature-dependent *I*–*V*, variable-frequency *C*–*V*, and Hall measurements, the effects of the thermal oxidation on the electrical properties of Ni/Au Schottky contacts on the $In_{0.18}Al_{0.82}N$/GaN heterostructures are investigated. A decrease of the reverse leakage current down to six orders of magnitude is observed after the thermal oxidation of bare $In_{0.18}Al_{0.82}N$/GaN heterostructures at 700 °C. It is confirmed that the reverse leakage current is dominated by F–P emission, and the main source of the leakage current is the emission of electrons from a trapped state near the M/S interface into a continuum of electronic states associated with the conductive dislocations in the $In_xAl_{1-x}N$ barrier. It is believed that the thermal oxidation results in the formation of a thin oxide layer on the $In_xAl_{1-x}N$ surface, which increases the emission barrier height from 0.003 ev to 0.34 eV. Therefore, the reverse leakage current is reduced significantly. It is suggested that the thermal oxidation is a simple and effective method of minimizing the reverse leakage current in $In_{0.18}Al_{0.82}N$/GaN HEMTs.

References

[1] Gonschorek M, Carlin J F, Feltin E, Py M A and Grandjean N 2006 *Appl. Phys. Lett.* **89** 062106
[2] Gadanecz A, Bläsing J, Dadgar A, Hums C and Krost A 2007 *Appl. Phys. Lett.* **90** 221906
[3] Kuzmík J, Kostopoulos A, Konstantinidis G, Carlin J F, Georgakilas A and Pogany D 2006 *IEEE Trans. Electron Devices* **53** 422
[4] Arslan E, Bütün S and Ozbay E 2009 *Appl. Phys. Lett.* **94** 142106
[5] Chikhaoui W, Bluet J M, Poisson M A, Sarazin N, Dua C and Bru-Chevallier C 2010 *Appl. Phys. Lett.* **96** 072107
[6] Zhang H, Miller E J and Yu E T 2006 *J. Appl. Phys.* **99** 023703
[7] Huang S, Shen B, Wang M J, Xu F J, Wang Y, Yang H Y, Lin F, Lu L, Chen Z P, Qin Z X, Yang Z J and Zhang G Y 2007 *Appl. Phys. Lett.* **91** 072109
[8] Levinshtein M, Rumyantsev S L and Shur M 2001 *Properties of Advanced Semiconductor Materials* (New York: Wiley) p. 2001
[9] Lin Y J, Lin W X, Lee C T and Chang H C 2006 *Jpn. J. Appl. Phys.* **45** 2505
[10] Beena D, Lethy K J, Vinodkumar R, Mahadevan P V P, Ganesan V, Phase D M and Sudheer S K 2009 *Appl. Surf. Sci.* **255** 8334
[11] Wang R X, Xu S J, Shi S L, Beling C D, Fung S, Zhao D G, Yang H and Tao X M 2006 *Appl. Phys. Lett.* **89** 143505
[12] Miller E J, Dang X Z, Wieder H H, Asbeck P M, Yu E T, Sullivan G J and Redwing J M 2000 *J. Appl. Phys.* **87** 8070
[13] Özdemir A F, Türüt A and Köçe A 2003 *Thin Solid Films* **425** 210
[14] Wang Y S, Zheng Y D and Zhang R 1990 *Journal of Nanjing University (Natural Sciences Edition)* **26** 211
[15] Soh C B, Chua S J, Lim H F, Chi D Z, Tripathy S and Liu W 2004 *J. Appl. Phys.* **96** 1341